ELSEVIER

Journal of Biomechanics 36 (2003) 951–959

JOURNAL OF BIOMECHANICS

www.elsevier.com/locate/jbiomech
www.JBiomech.com

Modeling the bifurcating flow in an asymmetric human lung airway

Y. Liu*, R.M.C. So, C.H. Zhang

Department of Mechanical Engineering, The Hong Kong Polytechnic University, Hung Hom, Kowloon, Hong Kong

Accepted 28 January 2003

Abstract

In a former paper, the inspiratory flow characteristics in a three-generation symmetric bifurcation airway have been numerically investigated using a control volume method to solve the fully three-dimensional laminar Navier-Stokes equations. The present paper extends the work to deal with asymmetric airway extracted from the 5th–11th branches of the model of Weibel (Morphometry of the Human Lung. New York Academic Press, Verlag, 1963) in order to more appropriately model human air passage. Computations are carried out in the Reynolds number range 200–1600, corresponding to mouth-air breathing rates ranging from 0.27 to 2.16 l/s, representative for an averaged height man breathing from quiet to vigorous state. Particular attentions are paid to establishing relations between the Reynolds number and the overall flow characteristics, including flow patterns and pressure drop. The study shows that the ratios of airflow rate through the medial branches to that of their mother branches are the same, and this is also true for the ratios of airflow rate through the lateral branches. This partially explains why regular human breathing is not affected by airways of different sizes.

Keywords: Asymmetric bifurcation flow; Human lung; Three-dimensional modeling

1. Introduction

The central airways of the lung are a complex system of branching tubes, a statistical analysis of human bronchial morphometry data (Raabe et al., 1976) revealed distinct asymmetric features of the airway branching pattern (Koblinger and Hofmann, 1985). Such an asymmetry in airway diameter, branching angle, and flow division could significantly affect the local distribution of particle deposition within airway bifurcations and ratios of air mass flow rate within daughter branches (Balashazy and Hofmann, 1995). Particularly, human lung airways are the most effective structure in which the mass flow rate in each branch should be balanced. An appreciation of their aerodynamic behavior is important to the understanding of their physiological role.

In order to understand this flow phenomenon, numerous studies on bifurcating flows have been carried out. Most of the studies have focused on the flow and deposition in a symmetric bifurcation model under symmetric flow conditions. From these studies (Schroter and Sudlow, 1969; Pedley et al., 1977; Isabey and Chang, 1981; Snyder and Olson, 1989; Zhao and Lieber, 1994), skewed velocity profiles and two symmetric eddies in the two-generation experimental bifurcation flow models were found. Finite element methods were used to numerically study the inspiratory and expiratory steady flows in a two-generation three-dimensional model (Zhao et al., 1997), the sixteenth-generation airway of the Weibel (1963) symmetric lung model (Gradon and Orlicki, 1990), and the three-generation, three-dimensional model (Liu et al., 2002).

In order to closely approximate airways in human lungs realistically, asymmetric air passages will have to be considered, but the number of investigations carried out on asymmetric bifurcation flows is extremely small. The studies of Kim and Iglesias (1989) and Kim et al. (1989) are two of the very few published experimental investigations in which the effect of asymmetry has been examined for inspiratory as well as expiratory flow conditions. Balashazy et al. (1991) and Balashazy and Hofmann (1995) analytically and numerically studied the effects of asymmetry in airway diameter, branching

*Corresponding author. Tel.: +852-2766-7814; fax: +852-2365-4703.

E-mail address: mmyliu@polyu.edu.hk (Y. Liu).

0021-9290/03/$ - see front matter
doi:10.1016/S0021-9290(03)00064-2

angle, and flow division on both inspiratory and expiratory flows. Unfortunately, their study only focused on a two-generation bifurcation. On the other hand, Zhang et al. (2000) numerically examined the effects of asymmetric branch flow rates on aerosol deposition in three-generation bifurcating airways. In their study, the geometry was symmetric but non-uniform outlet pressures were assigned to create asymmetric flow rate ratios. Comer et al. (2001a, b) used the same technique to calculate the flow structures and particle deposition patterns in three-generation airway models.

The present analysis extends the previous numerical work of Liu et al. (2002) to explore the effects of asymmetry in airway diameter and flow division on inspiratory flow for different flow rates. Since all conditions are those as previously reported by Liu et al. (2002), the present work allows accurate evaluation of the effects of asymmetry alone.

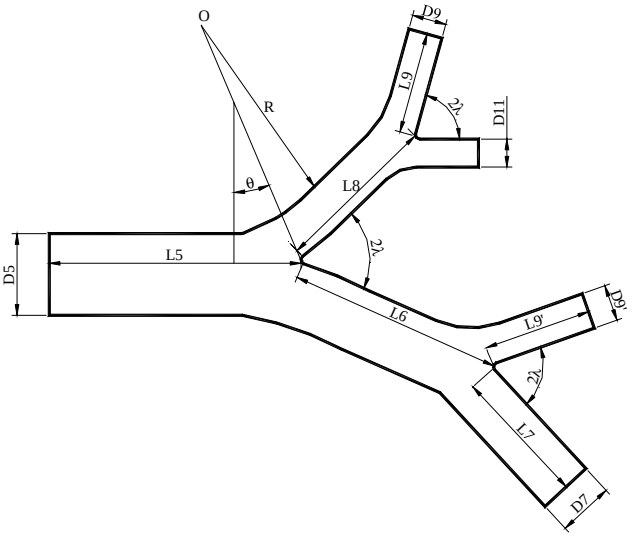

Fig. 1. Schematic view of the three-generation lung airway.

2. Numerical modeling

A schematic view of the asymmetric bifurcation model is given in Fig. 1 and a smooth wall is assumed. The geometric parameters represent airway generations from 5 to 11 after Weibel (1963). This asymmetric branching is from one mother tube to two unequal daughter tubes, where the lateral daughter tube is just the next generation of the mother tube and the medial daughter tube is three generations younger. The generating method of model geometry follows the definition of Zhao and Lieber (1994), and has been explained elsewhere (Liu et al., 2002). The geometric parameters are tabulated in Table 1. In Fig. 1 and Table 1, $L5-L11$ are the axial lengths and D_5-D_{11} are the diameters of the 5th–11th generations of Weibel's human lung model. Each branch tube is composed of a straight circular tube and a following straight asymmetrically elliptic tube of which the cross-sectional area is equal to that of the previous circular tube and the minor axes length b vary linearly from the diameter of the mother branch to the diameters of the daughter branches. The angle θ is chosen in such a way that the length of the divider occupies 2/3 of the length of the corresponding generation and the length of the daughter tube occupies 1/3 of the length of the next generation.

The Navier-Stokes and continuity equations in a three-dimensional mesh with a control volume approximation (Liu et al., 2002) are solved numerically to give the velocity field within the bifurcation. The boundary conditions for the governing equations are: (i) at the inlet of the grandmother branch (G5), the velocity field is characterized by a stationary parabolic profile; (ii) at the four outlets of the daughter branch, a uniform static pressure is specified; (iii) at the surface of the whole bifurcation, the no-slip boundary condition is invoked. The boundary condition at the outlet will affect the mass flow rate at bifurcation. To evaluate the influence of asymmetry bifurcation on flow rate, the back pressure of all the outlets has been set to zero, and the artifacts of the outlet boundary condition has been eliminated. An unstructured mesh with tetrahedral elements is used throughout, as shown in Fig. 2. The number of elements is about 123,591 for the airway. These numbers are determined by using different meshes, from coarse to progressively fine, until the calculated mass flow rates are mesh-convergent to within a prescribed tolerance ($\sim$0.5%). Details of the algorithm have been discussed elsewhere, the computer simulation model for airflow has been validated with experimental velocity data of Zhao and Lieber (1994) for a two-generation symmetric bifurcation (Liu et al., 2002); agreement between experimental and numerical results is excellent.

3. Results and discussion

The calculated velocity profiles, flow patterns, pressure drop and flow partition are discussed over a range of Reynolds number. The Reynolds number is defined as $Re_D = \rho U D_5/\mu$, where U is the mean velocity at the inlet tube, ρ is the air density and μ is the air dynamic viscosity. Computations are carried out for 8 different Re_D ranging from 200 to 1600. This range of Re_D is chosen to correspond to mouth-air breathing rates of 0.27–2.16 l/s, or an averaged height man breathing from a quiet to a vigorous state.

It should be pointed out that the real respiratory flow is a typical fluid–structure interaction problem. If this complicated fluid–structure interaction effect were to be accounted for, the walls of the tubes have to be

Table 1
Geometric parameters from the 5th–11th generation in the human lung model of Weibel (1963)

Generation in current model	Generation in Weibel's model	D (mm)	L (mm)	R (mm)	2λ (degree)
1st (Grand mother)	5	3.50	10.7		70
2nd (Mother)	6	2.80	9.0	$7D_6$	70
	8	1.86	6.4	$7D_8$	70
3rd (Daughter)	7	2.3	7.6	$7D_7$	70
	9	1.54	5.4	$7D_9$	70
	11	1.09	3.9	$7D_{11}$	70

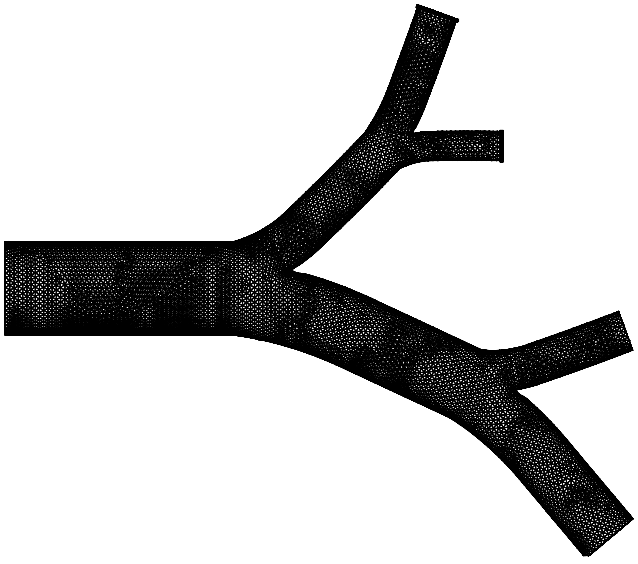

Fig. 2. Schematic views of the mesh.

considered elastic rather than rigid. Consideration of elastic walls is reserved for a future study after the asymmetry effect has been properly understood.

The discussion below is separated into four different sections. The first is on the flow patterns in the cross plane of the mother and daughter tubes, the second is on the velocity distributions from the first to the third-generation airways, the third is on the flow partitioning in the branches and the fourth is on the pressure drop behavior and their comparison with measurements.

3.1. Secondary flow pattern

The calculated flow patterns over the Re range investigated are quite similar. Therefore, only the results for $Re = 1600$ are shown in Fig. 3 to illustrate their general behavior at the middle of the different branches in the airways. At branch G6 and G8, a Dean-type secondary flow pattern is clearly identified. In these second-generation branches (Fig. 3a and d), the fluid in the middle of the airway moves along the diameter, impinges on the inner wall, and then turns to move outward along the top and bottom walls to merge at the outer wall of the tube. The flow from the top and bottom wall merges to form two counter-rotating vortices, which are similar to those in curved tubes (Dean, 1927, 1928). This will cause the axial velocity profile to skew towards the inner wall as will be discussed in Fig. 4. Two counter-rotating vortices are still discernible at the third-generation branch airway. However, the secondary flow is relatively weak at the lateral branch (G7 and G9) than at the medial branch (G9′ and G11). This can be seen from Figs. 3b,c,e and f, respectively. The reason for the relatively weaker secondary flow in the lateral branch is that the skewed velocity profile in the mother branches (G6 and G8) brings much of the fluid into the medial branches (G9′ and G11). Since the diameters of the lateral branches are larger than those of the medial branches, this attracts fluid into the lateral tubes and secures the relative balance of the volume flow rate between the lateral and medial branches. This fact will be made clearer when the flow partitioning is examined in detailed in Section 3.3. Thus, the secondary flow in the lateral branches is still clearly identifiable even though it is not very strong. One can deduce that, if the diameters of the medial and lateral branches were equal, i.e., for the symmetric bifurcation flow, the secondary flow in the lateral branches would be much weaker, as discussed in Liu et al. (2002).

3.2. Velocity distribution

The flow vectors at the bifurcation plane are plotted in Fig. 4 for $Re_D = 200$ (Fig. 4a) and 1600 (Fig. 4b). Mean inlet velocities at the corresponding Re_D are used to scale the axial velocities in order to clearly illustrate the Re_D effect on the velocity distribution.

In the bifurcation plane, the inlet velocity profile at the entrance of the G5 tube is parabolic, due to the prescribed boundary condition. As the flow approaches the asymmetric divider, the velocity vector profile slightly skews towards the airway G6, due to the asymmetry of the flow divider causing more fluid to flow towards the larger branch. Along the secondary-generation G8, a secondary flow induced by the curved

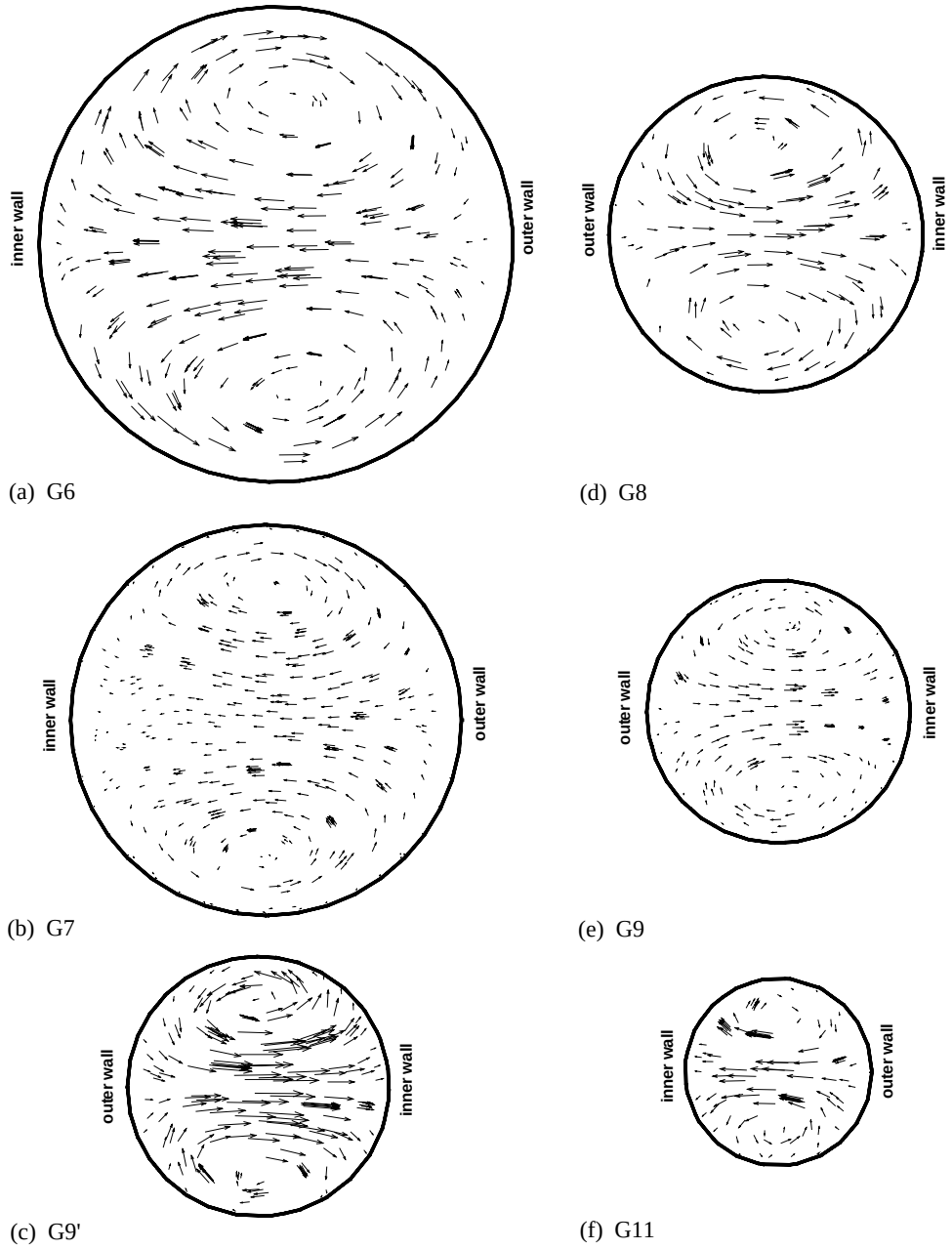

Fig. 3. Secondary flow vectors of asymmetric model at $Re = 1600$ in the middle of: (a) G6 branch, (b) G7 branch, (c) G9′ branch, (d) G8 branch, (e) G9 branch, and (f) G11 branch.

geometry drives air towards the inner wall of the bifurcation and the velocity profiles become skewed with the maximum velocity occurring near the inner wall (Fig. 3). The skewness increases with Re_D. As the flow approaches the second flow divider, i.e., in the outlet of the airway G8, the skewness in the profile for low Re_D begins to change and starts to skew towards the outer wall, but the profile for high Re_D remains essentially unchanged. The most likely explanation for this phenomenon is that as the fluid approaches the divider, it tends to flow towards the larger branch—G9; however, the secondary flow drives the fluid towards the inner wall, i.e., the side of the smaller branch—G11. For lower Re_D, the secondary flow is too weak to overcome the "attraction" of the larger branch. As Re_D increases, the secondary flow becomes stronger and stronger. At a certain Re_D, it is strong enough to keep the fluid near the inner wall, thus retaining the skewness as shown in the figure. Again due to the effect of curvature, along the entrance of airway G9, the velocity profile skews toward the inner wall.

A similar phenomenon can be found in the larger branch G6–G7–G9′. At the outlet of G6 just before the bifurcation carina, due to the "attraction" of the larger

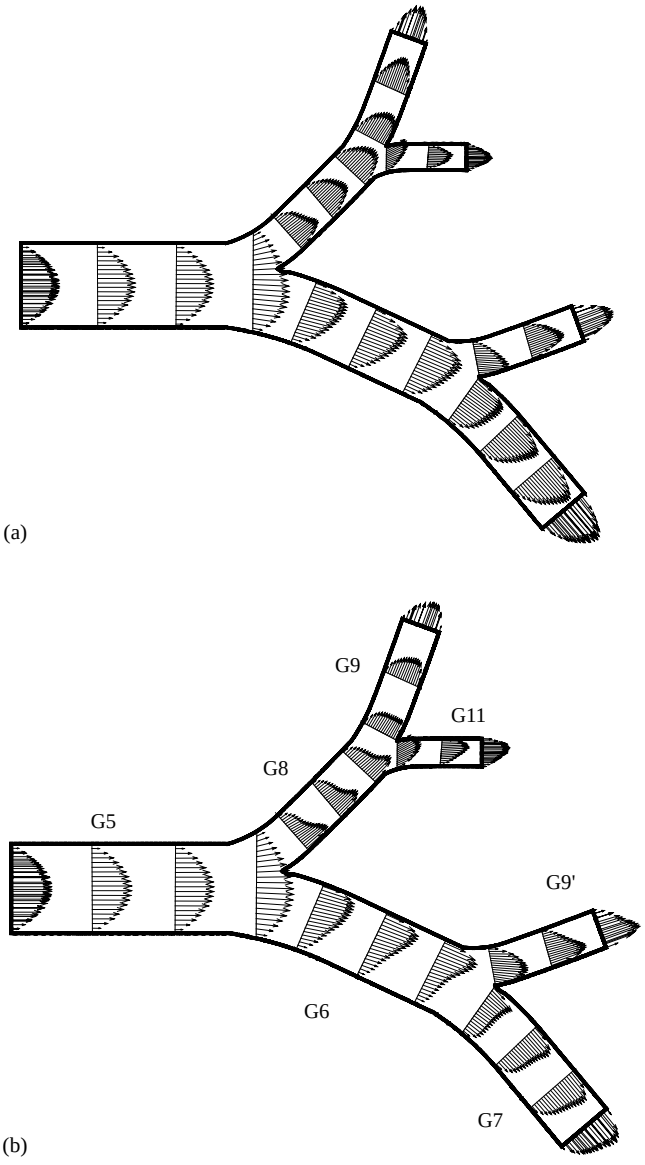

Fig. 4. Axial flow vectors at: (a) $Re_D = 200$, and (b) $Re_D = 1600$.

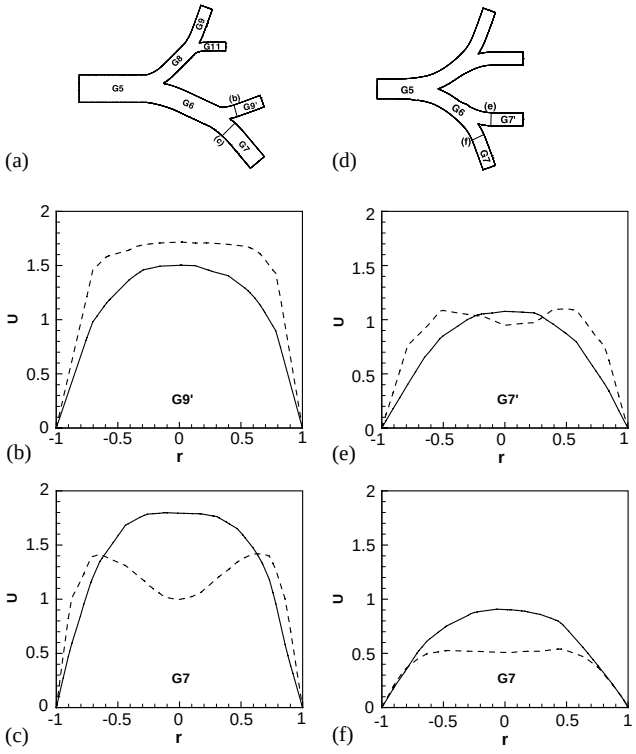

Fig. 5. Axial velocity profile in the transverse plane comparison between asymmetric and symmetric model in the third generation: (a) Schematic view of asymmetric model; (b) Velocity profile of asymmetric model in medial branch (G9′); (c) Velocity profile of asymmetric model in lateral branch (G7); (d) Schematic view of symmetric model; (e) Velocity profile of symmetric model in medial branch (G7′); (c) Velocity profile of symmetric model in lateral branch (G7). $Re_D = 200$ ——; $Re_D = 1600$ · · · · · · · ·.

branch, the velocity profiles for both Re_D seem to move toward the outer wall—the side of G7. However, after the carina, the skewness moves towards the inner wall again. Generally, due to the skewed velocity profile in the second generation, the fluid momentum per unit cross-sectional area in the medial branches (G11 and G9′) is higher than that in the lateral branches (G9 and G7) in the third generation.

Fig. 5 shows the comparison of velocity profile between asymmetric and symmetric airways in the transverse plane, which is perpendicular to the bifurcation plane. Again, mean inlet velocities at the corresponding Re_D are used to scale the axial velocities in order to clearly illustrate the Re_D effect on the velocity distribution. Generally, the velocity profile in the transverse plane after the bifurcation shows an M shape due to the strong secondary flow caused by streamline curvature, and this is true for the velocity profile in the second generation for both the symmetric and asymmetric airways, even though the velocity profiles are not plotted in Fig. 5. However, in the third-generation bifurcation airways the velocity profiles in the transverse plane are quite different. At lower Re_D, viscosity plays an important role; therefore, the profile remains essentially parabolic due to the relatively weaker secondary flow. At higher Re_D, for asymmetric airways, the velocity profile shows an almost parabolic shape in the medial branch-G9′, the smaller branch as shown in Fig. 5b. Even though the secondary flow in branch G9′ is very strong as indicated in Fig. 3, it is not strong enough to drive the high momentum fluid toward the wall of the tube, therefore the M-shape velocity profile cannot show up in G9′. In the lateral branch G7, the fluid momentum is not as high as in medial branch G9′, the secondary flow is weaker than that in G9′, as discussed in Fig. 3. However, due to its larger tube size, most of the fluid is attracted into G7, and the secondary flow is resulted from the relative high momentum fluid and curvature effect. This secondary flow is strong

enough to force the low momentum fluid toward the wall of the G7 tube, therefore the M-shape velocity profile is observed in the transverse plane as shown in Fig. 5c. For symmetric airways, most of the fluid is attracted into the medial branch (G7′) and the fluid momentum in the medial branch is much higher than that in the lateral branch (G7). Therefore the velocity profile is an M shape in the medial branch (Fig. 5e) and parabolic in the lateral branch (Fig. 5f).

3.3. Flow partitioning

In the second-generation bifurcation, the diameter of the G6 airway is much larger than that of the G8 airway. Consequently, more than half of the fluid will move into the G6 airway. Again, in the third-generation bifurcation, the skewed axial velocity in the second-generation airway and the asymmetric geometry in the third-generation airway will lead to an imbalance in the flow partition throughout the medial and lateral branches. This imbalance in flow partitioning can be measured by $\bar{m}$, which is defined as the ratio of the mass flow rate

$$\bar{m} = \frac{\dot{m}_i}{\dot{m}_j}, \tag{1}$$

where the indices i and j are used to denote the branch as indicated in Fig. 1. The mass flow rates are calculated by integrating the axial velocity profiles around the airway and the resulting plots of different $\bar{m}$ versus Re_D are shown in Fig. 6. Fig. 6a and b show the influence of Re_D on the ratios of the mass flow rate between daughter branches and grandmother airway G5. From Fig. 6a, it can be seen that about 26% of the total fluid is attracted into the G8 airway—the smaller branch, where m_5 is the mass flow rate of the G5 airway. In a symmetric bifurcation, the mass flow rate of the medial branch in the third-generation is usually much larger than that of the lateral branch due to the skewed axial velocity profile in the second-generation (Liu et al., 2002). However, in this asymmetric model, the lateral branch (G9) attracts much more fluid than the medial branch (G11), due in part to its larger diameter. In this analysis, the lateral branch G9 attracts about 18% of the total fluid in G5 and the medial branch (G11) attracts approximately 8%. With increasing Re_D, the mass flow rate increases slightly in branch G8 and the medial branch G11, but decreases slightly in the lateral branch G9. Basically, Fig. 6b shows the same trend in branch G6 and in its daughter branches G7 and G9′. Due to the much larger diameter of G6, up to 74% of the total fluid in G5 is attracted into branch G6. The mass flow rate in the lateral branch G7 takes about 50% of the total fluid and the medial branch G9′ receives only about 24%. The influence of Re_D on the flow rate in the G6 branch is stronger than that in G8.

Fig. 6c shows the ratio of mass flow rate between the same generation airways, i.e., between the two second-generation tubes G6 and G8, and between the two-third-generation tubes G9 and G11, and G7 and G9′. In the second generation, the mass flow rate in G6 is about three times that in G8. With increasing Re_D, the portion of G6 decreases slightly. In the third generation, although the size of the branches is different from each other, the ratio of the mass flow rate between the lateral and the medial branch is almost identical. As Re_D increases, the skewed axial velocity profile brings more fluid into the medial branches (G11 and G9′). Consequently, the ratio of the mass flow rate between the lateral and the medial branch decreases significantly. However, the ratio of the mass flow rate between the lateral and the medial branch still remains almost identical.

A comparison of the mass flow rate ratios between the third generation and their mother generation airways is shown in Fig. 6d. For different branches (branches G6 and G8), the mass flow rate ratios between the lateral daughter branches and their mother branches are almost equal, and the same is also true for the mass flow rate ratios between the medial daughter branches and their mother branches. This result is unexpected and raises the question of whether this is due to the ratio of the cross-sectional areas between mother and daughter tubes. In order to investigate the influence of cross-sectional area on the flow rate ratio, the various ratios between the branches are tabulated in Table 2 for comparison. From Table 2, the cross-sectional area roughly follows a geometric series, and this might partially explain the results shown in Fig. 6d. However, if the ratios of the medial daughter branches and their mother branches are considered, the discrepancy between the cross-sectional area ratios is as large as 13.5%, but the discrepancy of the mass flow ratios is only about 2.5%. This suggests that the axial velocity acts to equilibrate the mass flow rate ratios in spite of the difference in area ratios. Human lung is a very complicated and most optimal structure. It seems that this complication is built in to help even out human breathing. Another investigation is needed to further understand the full effect of the different generation branch combination.

3.4. Pressure drop behavior

Pressure drop in the bifurcating airways plays an important role in the respiratory process. The respiratory process can only take place continually and normally when the alternative contraction and expansion of the respiratory muscles overcomes the pressure drop due to viscous and other losses. In the present calculation, the dimensional pressure drop along the

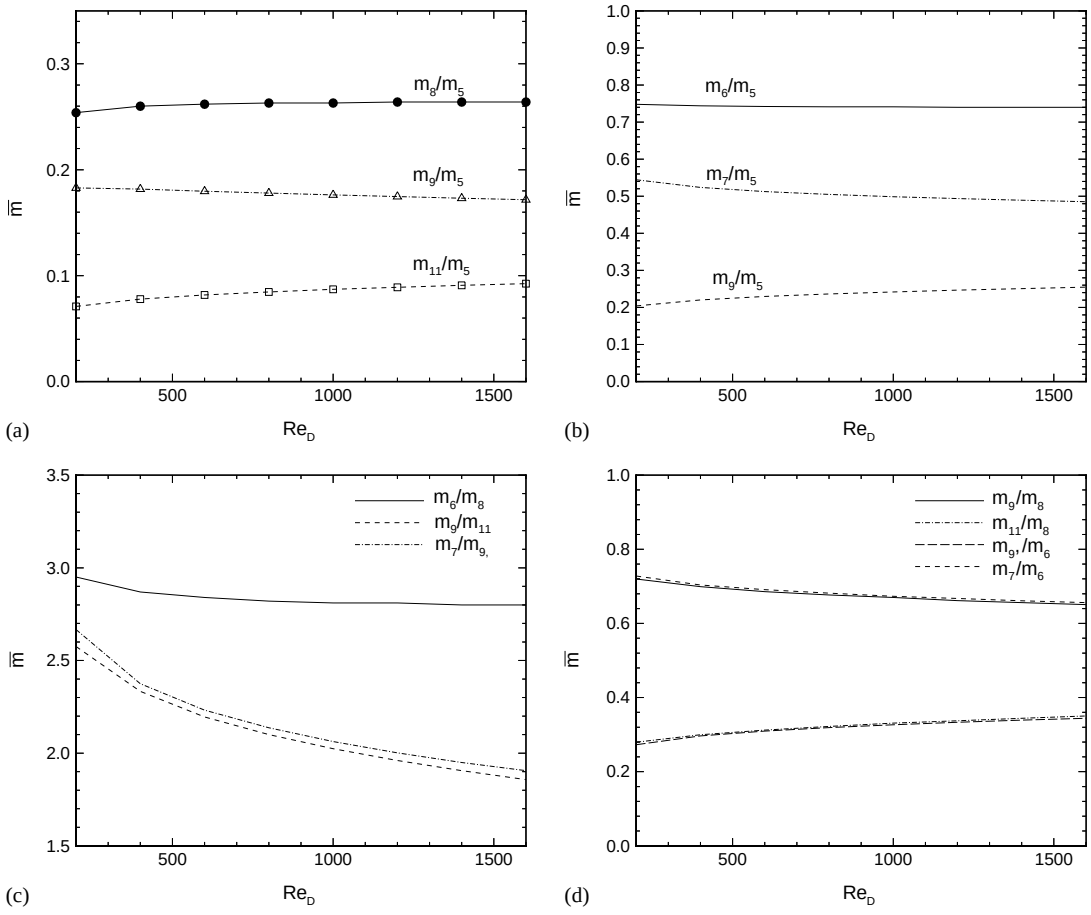

Fig. 6. Variation of the mass flow rate ratio, $\bar{m}$, with Re_D. (a) Between the upper daughter branches and grandmother airway G5, (b) between the lower daughter branches and grandmother airway G5, (c) between the branches of same generation, and (d) between the third generation branches and their mother branch.

Table 2
Ratios of cross sectional areas and mass flow rates

D_{11}^2/D_8^2	$D_{9'}^2/D_6^2$	Relative difference %	$Re = 200$			$Re = 1600$		
Medial daughter branch/Mother branch								
			m_{11}/m_8	$m_{9'}/m_6$	Relative difference (%)	m_{11}/m_8	$m_{9'}/m_6$	Relative difference (%)
0.3434	0.3025	13.5%	0.27953	0.27285	2.4%	0.3502	0.3443	1.7%
Lateral daughter branch/Mother branch								
D_9^2/D_8^2	D_7^2/D_6^2	Relative difference %	$Re = 200$			$Re = 1600$		
			m_9/m_8	m_7/m_6	Relative difference (%)	m_9/m_8	m_7/m_6	Relative difference (%)
0.6855	0.6747	1.6%	0.71995	0.72761	1.05%	0.6505	0.6559	0.8%

airways is defined as

$$\Delta P^* = (P_{\text{in, total}} - P_{\text{out, total}})\rho U^2, \tag{2}$$

where

$$P_{\text{in, total}} = \frac{\int_{A_{\text{in}}}(p + 0.5\rho(u^2 + v^2 + w^2))\rho\vec{V}\cdot \mathrm{d}\vec{A}_{\text{in}}}{\int_{A_{\text{in}}}\rho\vec{V}\cdot \mathrm{d}\vec{A}_{\text{in}}}, \tag{3}$$

$$P_{\text{out, total}} = \frac{\int_{A_{\text{out}}}(p + 0.5\rho(u^2 + v^2 + w^2))\rho\vec{V}\cdot \mathrm{d}\vec{A}_{\text{out}}}{\int_{A_{\text{out}}}\rho\vec{V}\cdot \mathrm{d}\vec{A}_{\text{out}}}. \tag{4}$$

In (3) and (4), $P_{\text{in,total}}$ is the mass-weighed integral of the total pressure over the inlet section of the first branch, and $P_{\text{out, total}}$ is the mass-weighted integral of the total pressure over the four outlet sections of the third branches. Here, A_{in} denotes the inlet

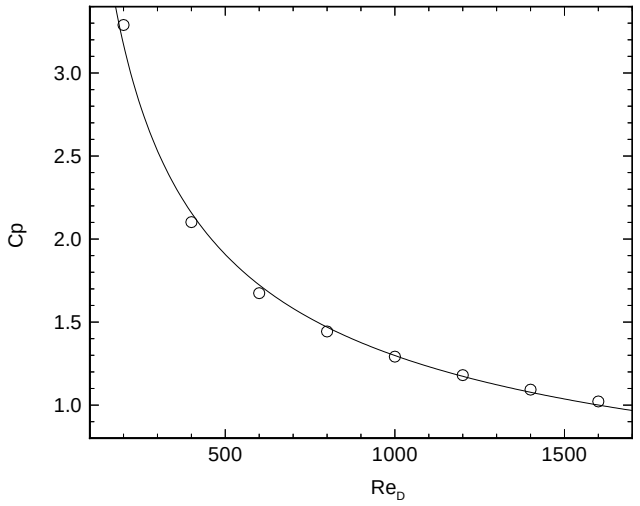

Fig. 7. Variation of the pressure drop coefficient C_p with Re_D.

cross-sectional area of the first branch and A_{out} denotes the four outlet cross-sectional areas of the third branch. The pressure drop coefficient C_p is defined as

$$C_p = \frac{\Delta P_{total}}{P_{in,\,dynamic}} = \frac{P_{in,\,total} - P_{out,\,total}}{P_{in,\,dynamic}}, \quad (5)$$

where

$$P_{in,\,dynamic} = \frac{\int_{A_{in}} 0.5\rho(u^2+v^2+w^2)\rho\vec{V}\cdot d\vec{A}_{in}}{\int_{A_{in}} \rho\vec{V}\cdot d\vec{A}_{in}}, \quad (6)$$

is the mass-weighed integral of the total pressure over the inlet section of the first branch.

Experimentally, it has been determined that $C_p \propto Re_D^{-0.5}$ in the central bronchi (Slutsky et al., 1980; Isabey and Chang, 1981; Snyder and Olson, 1989; Pedley and Kamm, 1991). The present calculated asymmetric results of C_p versus Re_D are plotted in Fig. 7. The relation between C_p and Re_D can be fitted by

$$C_p = 59.9 Re_D^{-0.55}. \quad (7)$$

This relation is valid for the Re_D range, $200 < Re_D < 1600$. In spite of the fact that the human lung has air passages of different sizes and the geometry is asymmetric, the pressure drop behavior is not affected by this asymmetry and the more amazing thing is that the mass flow rate ratios between the medial daughter branches and their mother branches are essentially identical. Consequently, human breathing is uniform and regular even under very strenuous conditions.

4. Conclusions

Three-dimensional inspiratory flow in a three-generation asymmetric lung airway is numerically studied using a control volume method. The method has previously been validated against both numerical simulation and experimental measurements and good agreement was obtained. The computations have been carried out at eight different Re_D ranging from 200 to 1600. The numerical results obtained lead to the following conclusions:

1. In this asymmetric model, the mass flow rate ratio between the medial branch in the third generation and their mother branch is essentially the same, and this is also true for the lateral tubes in the third generation. Since this asymmetric arrangement follows some order as described in Section 2, this raises the issue of whether the same phenomenon could also be observed for a different asymmetric arrangement? This deserves further study.
2. For a symmetric bifurcation, the secondary flow in the lateral branch is very weak. In this asymmetric model, due to the larger size of the lateral branches, most of the fluid has been attracted into the lateral tubes in the third bifurcation. Consequently, the secondary flow in the lateral branches of the third bifurcation has been enhanced significantly compare to the symmetric bifurcation.

Acknowledgements

Support given by the Research Grants Council of the Government of the HKSAR under Grant No. PolyU 5166/01E and 5172/02E and by the Hong Kong Polytechnic University under Central Research Grant No. A-PD75 is gratefully acknowledged.

References

Balashazy, I., Hofmann, W., 1995. Deposition of aerosols in asymmetric airway bifurcations. Journal of Aerosol Science 26, 273–292.

Balashazy, I., Hofmann, W., Martonen, T.B., 1991. Inspiratory particle deposition in airway bifurcation models. Journal of Aerosol Science 22, 15–30.

Comer, J.K., Kleinstreuer, C., Zhang, Z., 2001a. Flow structures and particle deposition patterns in double-bifurcation airway models. Part 1. Air flow fields. Journal of Fluid Mechanics 435, 25–54.

Comer, J.K., Kleinstreuer, C., Kim, C.S., 2001b. Flow structures and particle deposition patterns in double-bifurcation airway models. Part 2. Aerosol transport and deposition. Journal of Fluid Mechanics 435, 55–80.

Dean, W.R., 1927. Note on the motion of fluid in a curved pipe. Philosophical Magazine 4 (Suppl. 7), 208–223.

Dean, W.R., 1928. The streamline motion of fluid in a curved pipe. Philosophical Magazine 5 (Suppl. 5), 674–695.

Gradon, L., Orlicki, D., 1990. Deposition of inhaled aerosol particles in a generation of the tracheobronchial tree. Journal of Aerosol Science 21, 1–9.

Isabey, D., Chang, H.K., 1981. Steady and unsteady pressure-flow relationships in central airways. Journal of Applied Physiology 51, 1338–1348.

Kim, C.S., Iglesias, A.J., 1989. Deposition of inhaled particles in bifurcating airway models: I. Inspiratory deposition. Journal of Aerosol Medicine 2, 1–14.

Kim, C.S., Iglesias, A.J., Garcia, L., 1989. Deposition of inhaled particles in bifurcating airway models: II. Expiratory deposition. Journal of Aerosol Medicine 2, 15–27.

Koblinger, L., Hofmann, W., 1985. Analysis of human lung morphometric data for stochastic aerosol deposition calculations. Physics in Medicine and Biology 30, 541–556.

Liu, Y., So, R.M.C., Zhang, C.H., 2002. Modeling the bifurcating flow in a human lung airway. Journal of Biomechanics 35, 477–485.

Pedley, T.J., 1977. Pulmonary fluid dynamics. Annual Review of Fluid Mechanics 9, 229–274.

Pedley, T.J., Kamm, R., 1991. Dynamics of gas flow and pressure-flow relationships. In: Crystal, R., West, J. (Eds.), The Lung: Scientific Fundations. Raven Press Ltd., New York, pp. 995–1010.

Raabe, O.G., Yeh, H.C., Schum, G.M., Phalen, R.F., 1976. Tracheobronchial geometry: human, dog, rat, hamster. Lovelace Foundation Report LF-53.

Schroter, R.C., Sudlow, M.F., 1969. Flow patterns in models of the human bronchial airways. Respiratory Physiology 7, 341–355.

Slutsky, A., Berdine, G., Drasen, J., 1980. Steady flow in a model of human central airways. Journal of Applied Physiology 49, 417–423.

Snyder, B., Olson, D.E., 1989. Flow development in a model airway bronchus. Journal of Fluid Mechanics 207, 378–392.

Weibel, E.R., 1963. Morphometry of the Human Lung. Springer, Academic Press, Berlin, New York.

Zhang, Z., Kleinstreuer, C., Kim, C.S., 2000. Effects of asymmetric branch flow rates on aerosol deposition in bifurcating airways. Journal of Medical Engineering and Technology 24, 192–202.

Zhao, Y., Lieber, B.B., 1994. Steady inspiratory flow in a model symmetric bifurcation. ASME Journal of Biomechanical Engineering 116, 488–496.

Zhao, Y., Brunskill, C.T., Lieber, B.B., 1997. Inspiratory and expiratory steady flow analysis in a model symmetrically bifurcating airway. ASME Journal of Biomechanical Engineering 119, 52–58.